AGU PUBLICATIONS

Geophysical Research Letters

RESEARCH LETTER
10.1002/2017GL075433

Key Points:
- Our new data show a reduced amplitude of El Nino events during the early and mid-Holocene
- Overall, proxy data supports both a June insolation-forced trend in ENSO strength and decadal-centennial variability in ENSO strength
- The best supported mechanism for insolation forcing of Holocene ENSO is a weaker upwelling feedback, due to a warmer/deeper thermocline

Supporting Information:
- Supporting Information S1

Correspondence to:
S. M. White,
smwhite@ucsc.edu

Citation:
White, S. M., Ravelo, A. C., & Polissar, P. J. (2018). Dampened El Niño in the early and mid-Holocene due to insolation-forced warming/deepening of the thermocline. *Geophysical Research Letters*, *45*, 316–326. https://doi.org/10.1002/2017GL075433

Received 25 AUG 2017
Accepted 15 DEC 2017
Accepted article online 19 DEC 2017
Published online 8 JAN 2018

©2017. American Geophysical Union. All Rights Reserved.

Dampened El Niño in the Early and Mid-Holocene Due To Insolation-Forced Warming/Deepening of the Thermocline

Sarah M. White[1], A. Christina Ravelo[2], and Pratigya J. Polissar[3]

[1]Department of Earth and Planetary Sciences, University of California, Santa Cruz, CA, USA, [2]Department of Ocean Sciences, University of California, Santa Cruz, CA, USA, [3]Department of Biology and Paleoenvironment, Lamont Doherty Earth Observatory of Columbia University, Palisades, NY, USA

Abstract El Niño–Southern Oscillation (ENSO) dominates interannual climate variability; thus, understanding its response to climate forcing is critical. ENSO's sensitivity to changing insolation is poorly understood, due to contrasting interpretations of Holocene proxy records. Some records show dampened ENSO during the early to mid-Holocene, consistent with insolation forcing of ENSO amplitude, but other records emphasize decadal-centennial fluctuations in ENSO strength, with no clear trend. To clarify Holocene ENSO behavior, we collected proxy data spanning the last ~12 kyr and find relatively low El Niño amplitude during the early to mid-Holocene. Our data, together with published work, indicate both a long-term trend in ENSO strength due to June insolation forcing and high-amplitude decadal-centennial fluctuations; both behaviors are shown in models. The best supported mechanism for insolation-driven dampening of ENSO is weakening of the upwelling feedback by insolation-forced warming/deepening of thermocline source waters. Elucidating the thermocline's role will help predict future ENSO change.

1. Introduction

El Niño–Southern Oscillation (ENSO) is a key source of interannual climate variability, with global impacts including drought, floods, coral bleaching, and decreased fisheries yield. It remains uncertain whether ENSO will strengthen or weaken in response to anthropogenic climate change (Christensen et al., 2013), due in part to a lack of understanding of ENSO's sensitivity to external forcing and tropical Pacific mean climate. This ambiguity stems from contrasting conclusions drawn from Holocene proxy reconstructions of ENSO. Many reconstructions, including those derived from individual foraminifera, precipitation-sensitive indices, and corals/mollusks, show early and mid-Holocene dampening of ENSO; that is, El Niño and La Niña events had a lower amplitude and/or were less frequent relative to the late Holocene (Chen et al., 2016; Conroy et al., 2008; Driscoll et al., 2014; Duprey et al., 2012; Koutavas & Joanides, 2012; McGregor et al., 2013; McGregor & Gagan, 2004; Moy et al., 2002; Rodbell et al., 1999; Sadekov et al., 2013; Thompson et al., 2017; Tudhope et al., 2001; Woodroffe, 2003; Zhang et al., 2014). These reconstructions implicate external forcing of ENSO amplitude by insolation. However, recent compilations of many coral/mollusk records depict a Holocene ENSO history dominated by decadal-centennial fluctuations, similar to that of the last millennium (Cobb et al., 2003), with no long-term trend in ENSO strength attributable to insolation forcing (Cobb et al., 2013; Emile-Geay et al., 2016). In contrast to the divergent interpretations of proxy data, modeling studies are unanimous in finding that changing insolation dampened ENSO during the early and mid-Holocene (e.g., An & Choi, 2014; Braconnot et al., 2012; Bush, 2007; Chiang et al., 2009; Clement et al., 2000; Liu et al., 2014; Otto-Bliesner et al., 2003; Roberts et al., 2014) while also showing high-amplitude decadal-centennial variability in ENSO strength throughout the Holocene (Liu et al., 2014) similar to coral/mollusk reconstructions (Cobb et al., 2013; Emile-Geay et al., 2016). Although model studies agree that changes in insolation dampened ENSO during the early and mid-Holocene, they disagree on the mechanism. To validate model results, it is first necessary to develop a consensus view on Holocene ENSO behavior. If the balance of proxy data show a long-term trend in ENSO strength consistent with insolation forcing, then the mechanism by which insolation dampened ENSO can be assessed.

To determine whether there was a long-term trend in Holocene ENSO strength, we reconstructed temperature variability from individual foraminifera from the central equatorial Pacific during the Younger Dryas (YD) and the Holocene, filling key data gaps. Our new findings, together with published studies, provide strong

19448007, 2018, 1, Downloaded from https://agupubs.onlinelibrary.wiley.com/doi/10.1002/2017GL075433, Wiley Online Library on [19/07/2025]. See the Terms and Conditions (https://onlinelibrary.wiley.com/terms-and-conditions) on Wiley Online Library for rules of use; OA articles are governed by the applicable Creative Commons License

evidence for a long-term trend of dampened ENSO during the early to mid-Holocene, consistent with insolation forcing, superimposed on high-amplitude decadal-centennial fluctuations in ENSO strength. This interpretation reconciles apparently divergent reconstructions of Holocene ENSO and is consistent with model results. To test model-derived mechanisms for insolation-driven dampening of ENSO, we synthesized proxy data on Holocene tropical Pacific mean climate. We find that a weakened upwelling feedback, stemming from insolation-driven warming/deepening of the equatorial Pacific thermocline, is the best supported mechanism for early and mid-Holocene ENSO dampening.

2. Methods and Approach

2.1. Study Site

We used marine sediment cores MGL1208-14MC and 12GC (0°S, 156°W, 3,049 m depth) from the central equatorial Pacific, near the Line Islands (Figure S1 in the supporting information), where the mixed layer is ~100 m deep and the thermocline is at ~150 m (Figure S2). Our site is ideal for studying ENSO; the seasonal cycle amplitude in the mixed layer is only ±0.4°C, whereas the average peak sea surface temperature (SST) anomaly during El Niño events is +2°C (Carton & Giese, 2008). Therefore, ENSO dominates SST variability at our site, unlike locations farther east (Thirumalai et al., 2013) (Figure S1). The modern SST distribution, based on the past 50 years of data (the Simple Ocean Data Assimilation (SODA) v2.1.6 data set; Carton & Giese, 2008), shows that the warmest temperatures occur exclusively during El Niño events; seasonal variations are confined to the middle of the distribution. Further advantages of the site are that it lies within the Niño3.4 region, where ENSO events are defined (Trenberth, 1997), and enables side-by-side comparison to Line Islands coral records (e.g., Cobb et al., 2013).

2.2. Analytical Approach

To reconstruct El Niño amplitude, we acquired Mg/Ca-based temperatures from individual tests of *Globigerinoides sacculifer* without sac-like final chamber (hereafter referred to as *G. sacculifer*), a mixed-layer-dwelling foraminifer. We also measured Mg/Ca of pooled tests of *G. sacculifer* through the Holocene and late deglaciation, to elucidate average mixed-layer temperatures at the site. Foraminiferal Mg/Ca was converted to SST using the Anand et al. (2003) multispecies calibration with the Regenberg et al. (2014) multispecies dissolution correction, assuming modern ΔCO_3^{2-}. Radiocarbon dates were generated for every interval with individual foraminiferal data. See supporting information for details.

Foraminifera capture ~1 month "snapshots" of their environment, so by measuring 70–90 individuals from each sample, we reconstructed a distribution of SST representing monthly variability during seven time periods. Bioturbation broadens the time interval represented in each sample to ~800 years, given a 5 cm bioturbation depth (Trauth et al., 1997). To compare the SST distribution in each downcore interval to that of the core top, we use quantile-quantile plots, following the method of Ford et al. (2015). Quantile-quantile plots allow visual isolation and comparison of certain parts of the distribution, enabling separation of ENSO-related variability from seasonality, which is impossible with a simple metric such as standard deviation. A distribution with less extreme warm temperatures (i.e., the warmest temperatures are not as far above the mean) indicates lower amplitude of El Niño events, relative to the core top. To highlight differences in the warmest quantiles, downcore quantile data are normalized to the core top distribution (Figure S3 and supporting information).

3. Results

3.1. Comparison of Core Top *G. sacculifer* Temperatures to Benchmark Data Sets

Individual *G. sacculifer*-derived temperatures from the core top (dated to 4,030 years B.P.) agree with the modern temperature distribution in the mixed layer at our site (Carton & Giese, 2008) (Figures 1 and S4 and supporting information). This agreement implies that any bias from vertical migration or seasonal preference of the foraminifera is small. Our core top data are also similar to contemporaneous coral data from nearby Christmas Island (Cobb et al., 2013) (Figure S5 and supporting information), enabling direct comparison of the data sets. To minimize systematic biases in *G. sacculifer* temperatures due to bioturbation and other processes, we present all downcore data as deviations from the core top rather than the modern SST distribution. Confidence intervals are estimated by resampling the empirical continuous distribution function of each sample using a Monte Carlo simulation (see supporting information for details).

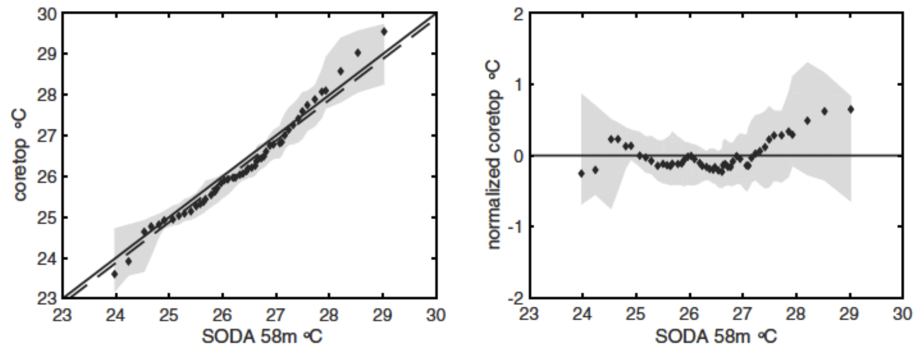

Figure 1. (left) Quantile-quantile and (right) normalized quantile-quantile plots of modern monthly gridded temperatures in the middle of the mixed layer (58 m depth) near our site, (the SODA v2.1.6 data set; Carton & Giese, 2008), plotted versus individual *G. sacculifer* temperatures from the core top. The core top matches the modern temperature distribution within 90% confidence intervals (gray region).

3.2. Sensitivity Tests

Sensitivity tests, performed by manipulating modern temperatures from the SODA data set (Carton & Giese, 2008) and subsampling them, show that our method can detect a decrease in El Niño amplitude as small as 20%, within 90% confidence intervals, and that even a 50% decrease in seasonal cycle amplitude does not affect the warmest quantiles. We also find that our observed trend in El Niño amplitude is unlikely to have arisen from random sampling of decadal-centennial variability in either ENSO strength (as described by Wittenberg, 2009) or in annual mean temperature (as described for the Line Islands region by Cobb et al., 2003) in the absence of a true long-term trend (Figures S6–S8 and supporting information).

3.3. Downcore Temperature Data

There is a clear trend in our individual foraminiferal data: the late Holocene and YD intervals are similar to the core top, whereas the five early and mid-Holocene intervals have less extreme warm temperatures, significant at the 90% confidence level, indicating reduced El Niño amplitude (Figure 2). These findings remain significant at the 80% confidence level after accounting for 0.4°C uncertainty in each data point, which stems from instrumental uncertainty, intratest variations, differential dissolution, and changes in salinity (Figure S9 and supporting information). Our findings remain similarly significant if we use the late Holocene sample as the baseline for comparison, instead of the core top (Figure S10). Long-term average Mg/Ca-derived SST estimates at our site show similar trends to those from the east equatorial Pacific (EEP), with slightly lower temperatures in the mid-Holocene relative to the early Holocene (Figure S11).

4. The Holocene History of ENSO

Our finding of reduced El Niño amplitude during the early and mid-Holocene, compared to the late Holocene and YD, is best evaluated in the context of previously published data and model studies, which are synthesized and presented in the following sections. Data (Table S3) from individual foraminifera, precipitation records, and corals/mollusks are consistent with models indicating both high-amplitude decadal-centennial fluctuations and a long-term trend in ENSO strength (Liu et al., 2014) and therefore provide evidence of insolation forcing of ENSO.

4.1. Individual Foraminiferal Records

Individual foraminiferal data in the EEP (Koutavas & Joanides, 2012) show strongly dampened ENSO in the mid-Holocene but more variability in ENSO strength during the early Holocene. This early Holocene variability was originally interpreted to indicate enhanced ENSO strength; however, it can also be explained by greater decadal-centennial variability in ENSO strength (section 4.3) superimposed on dampened ENSO on average, which agrees with similar data from a nearby site (Sadekov et al., 2013). Eastern tropical Pacific warm pool subsurface temperatures show slightly dampened variability in the early Holocene, albeit not statistically significant (Leduc et al., 2009). In any case, these subsurface data do not contradict our results since a deeper thermocline (section 5.1) can alter subsurface variability independently of changes in ENSO. In general,

19448007, 2018, 1, Downloaded from https://agupubs.onlinelibrary.wiley.com/doi/10.1002/2017GL075433, Wiley Online Library on [19/07/2025]. See the Terms and Conditions (https://onlinelibrary.wiley.com/terms-and-conditions) on Wiley Online Library for rules of use; OA articles are governed by the applicable Creative Commons License

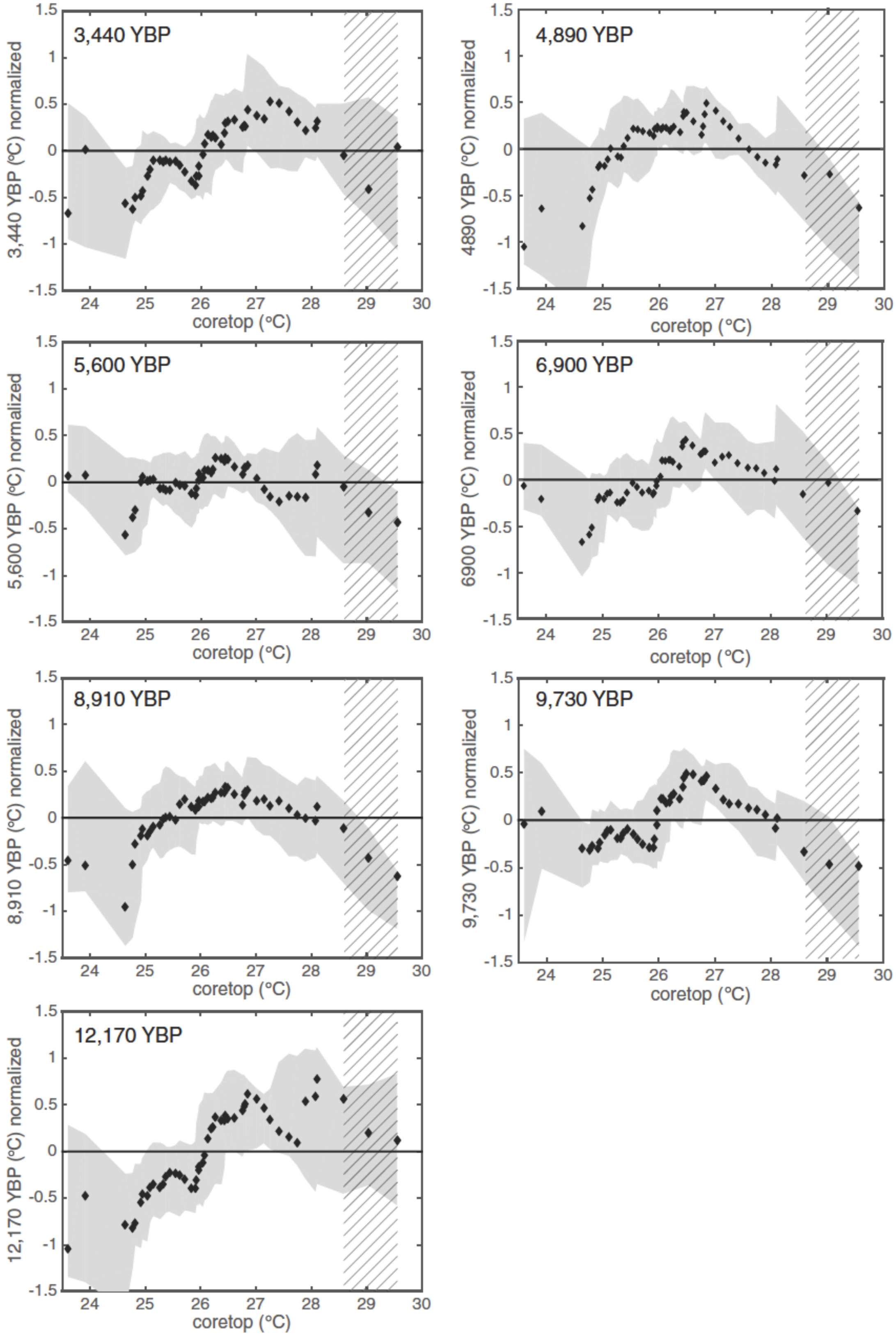

Figure 2. Mixed-layer temperature distributions from seven time intervals during the Holocene and YD at the Line Islands. Normalized quantile-quantile plots show the difference of each downcore quantile from the core top quantile (*y* axis) versus the core top quantiles (*x* axis). Patterned region highlights quantiles attributed solely to El Niño events, where points below the zero line indicate reduced amplitude of El Niño events. Gray shaded region indicates 90% confidence intervals.

19448007, 2018, 1, Downloaded from https://agupubs.onlinelibrary.wiley.com/doi/10.1002/2017GL075433, Wiley Online Library on [19/07/2025]. See the Terms and Conditions (https://onlinelibrary.wiley.com/terms-and-conditions) on Wiley Online Library for rules of use; OA articles are governed by the applicable Creative Commons License

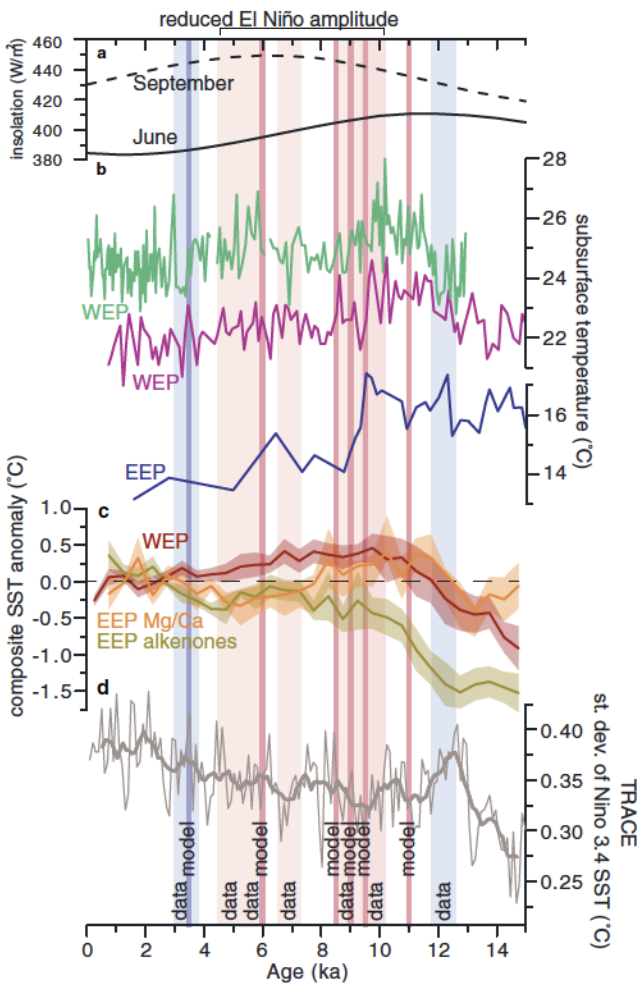

Figure 3. Reconstructions of ENSO in the context of model results, thermocline temperatures, and composite SST records from the WEP and EEP. Wide shaded bars show sample intervals from this study, each spanning ~800 years; pink/blue indicate lower/similar amplitude El Niño events, respectively, to the core top. Narrow bars show modeling results; dark pink/dark blue show reduced/similar ENSO to preindustrial, from modeling studies at 3.5 ka (Otto-Bliesner et al., 2003), 6 ka (An & Choi, 2014; Bush, 2007; Chiang et al., 2009; Otto-Bliesner et al., 2003), 8.5 ka (Otto-Bliesner et al., 2003; Roberts et al., 2014), 9 ka (Bush, 2007), 9.5 ka (Braconnot et al., 2012), and 11 ka (Otto-Bliesner et al., 2003), respectively. (a) September (dashed) and June (solid) insolation at the equator (Berger, 1978). (b) Subsurface temperatures from *P. obliquiloculata* Mg/Ca in the WEP (light blue, Dang et al., 2012; and purple, Xu et al., 2008), and *N. dutertrei* Mg/Ca in the EEP (dark blue; Sadekov et al., 2013). (c) Composite SST anomalies (with respect to average temperature 0–4 ka) from WEP Mg/Ca and coral Sr/Ca records (dark red), EEP Mg/Ca records (orange), and EEP alkenone records (olive green). Colored regions denote standard deviation of temperatures from all composited records. (d) Transient model run forced with insolation, CO_2, meltwater, and ice sheets, showing standard deviation of SST in the Nino3.4 box band-pass filtered at 1.5–7 years (Liu et al., 2014) (thin gray line), and 700 year smoothed model data (thick gray line).

individual foraminiferal records are consistent with dampened ENSO during the early to mid-Holocene, in agreement with our findings, and support insolation forcing of ENSO.

4.2. Precipitation-Based Records

Records of El Niño-related precipitation all show dampened El Niño in the mid-Holocene (Chen et al., 2016; Conroy et al., 2008; Moy et al., 2002; Rodbell et al., 1999; Thompson et al., 2017; Zhang et al., 2014). Some show dampened El Niño through the entire early and mid-Holocene (Moy et al., 2002; Rodbell et al., 1999) or very dampened El Niño in the mid-Holocene and moderately dampened El Niño in the early Holocene (Chen et al., 2016), but a few studies from a Galapagos lake indicate that El Niño was not dampened in the early Holocene (Conroy et al., 2008; Zhang et al., 2014). Overall, for the mid-Holocene, precipitation-based El Niño records agree with our results, but for the early Holocene, these records disagree among themselves and (in some cases) with our data, likely due to greater non-ENSO-related precipitation variability in the early Holocene caused by meltwater forcing (Bush, 2007; Liu et al., 2014) (section 4.4). As such, precipitation data do not contradict dampened ENSO during both the early and mid-Holocene.

4.3. Coral and Mollusk Records

Several coral and mollusk records, which provide decades-long, monthly resolved records of ENSO from discrete time intervals, show dampened ENSO in the early and mid-Holocene (Carre et al., 2014; Driscoll et al., 2014; Duprey et al., 2012; McGregor et al., 2013; McGregor & Gagan, 2004; Tudhope et al., 2001; Woodroffe, 2003). However, compilations of many such records depict a more complex picture, with substantially dampened ENSO from ~3–5 ka, and dampened ENSO on average but more record-to-record variability in ENSO strength during the early Holocene, which was argued to be inconsistent with a long-term trend in ENSO strength (Cobb et al., 2013; Emile-Geay et al., 2016). The record-to-record variability likely reflects decadal-centennial variations in ENSO strength, as shown in proxy data from the last millennium (Cobb et al., 2013) and in unforced model runs (Wittenberg, 2009; Wittenberg et al., 2014). These unforced short-term fluctuations were likely present throughout the Holocene and may have been of similar magnitude to a long-term trend in ENSO strength from insolation forcing (Liu et al., 2014, shown in Figure 3d), making detection of a trend difficult (Liu et al., 2014). In addition, there may have been forced decadal-centennial fluctuations in ENSO strength during the early Holocene (section 4.4), further hampering detection of a trend. Overall, the coral data can be interpreted as showing dampened ENSO on average during the early to mid-Holocene relative to the late Holocene, consistent with insolation forcing, combined with superimposed decadal-centennial variability in ENSO strength. These two behaviors are not mutually exclusive; both are shown in models (Liu et al., 2014).

4.4. Decadal-Centennial Forcings of ENSO Strength During the Early Holocene

Some of the observed decadal-centennial variability in early Holocene ENSO strength may have been forced by changing meltwater (Braconnot et al., 2012; Liu et al., 2014) or total solar irradiance (Marchitto et al., 2010). Models find that increased meltwater in the North Atlantic strengthens ENSO (Braconnot et al., 2012; Liu et al.,

19448007, 2018, 1, Downloaded from https://agupubs.onlinelibrary.wiley.com/doi/10.1002/2017GL075433, Wiley Online Library on [19/07/2025]. See the Terms and Conditions (https://onlinelibrary.wiley.com/terms-and-conditions) on Wiley Online Library for rules of use; OA articles are governed by the applicable Creative Commons License

2014; Timmermann et al., 2007). At 10 ka, sea level was ~40 m lower than today (Bard et al., 1996), so meltwater pulses in the early Holocene could have created decadal-centennial periods of strengthened ENSO superimposed on a long-term insolation-forced dampening of ENSO. Meltwater pulses would also disrupt teleconnections between precipitation-sensitive proxies in the eastern Pacific (Conroy et al., 2008; Zhang et al., 2014) and Nino3.4 SST, creating an increase in precipitation variability unrelated to ENSO (Liu et al., 2014). Another potential source of decadal-centennial forcing is total solar irradiance, which varied more in the early Holocene than the mid- to late Holocene (Marchitto et al., 2010). Changing solar irradiance is theoretically capable of affecting ENSO via ocean dynamical cooling (Emile-Geay et al., 2007) and is correlated with centennial-scale variations in early Holocene ENSO (Marchitto et al., 2010). Overall, the apparent increase in decadal-centennial variability in early Holocene ENSO strength shown in coral/mollusk records (Cobb et al., 2013; Emile-Geay et al., 2016) is likely an accurate representation of ENSO's behavior in response to a range of forcings. However, these short-term fluctuations cannot be taken as evidence for the lack of a long-term insolation-forced trend.

4.5. Model Results

Model studies are unanimous in simulating dampened ENSO during the early and mid-Holocene (e.g., An & Choi, 2014; Braconnot et al., 2012; Bush, 2007; Chiang et al., 2009; Clement et al., 2000; Otto-Bliesner et al., 2003; Pausata et al., 2017; Roberts et al., 2014). Model results from discrete time intervals are reported relative to preindustrial conditions, whereas our data are reported relative to the core top (Figure 3). Despite the difference in baseline, our findings are consistent with model results because both fall on a Holocene-long trend in ENSO strength (Figure 3d; Liu et al., 2014), in which both the early and mid-Holocene had dampened ENSO compared to our two youngest samples. The Liu et al. (2014) results also show high-amplitude decadal-centennial variations in ENSO strength. Overall, model results are consistent with Holocene proxy data in showing a long-term trend in ENSO strength due to insolation forcing, superimposed on short-term fluctuations in ENSO strength. Importantly, models show that these different scales of variability are not mutually exclusive.

5. Mechanism of Observed Trend in Holocene ENSO Strength

In general, Holocene proxy data show dampened ENSO in the early to mid-Holocene relative to the late Holocene, consistent with insolation forcing of ENSO. This interpretation agrees with numerous modeling and proxy studies (e.g., An & Choi, 2014; Braconnot et al., 2012; Bush, 2007; Chen et al., 2016; Chiang et al., 2009; Clement et al., 2000; Koutavas & Joanides, 2012; Liu et al., 2014; McGregor & Gagan, 2004; Otto-Bliesner et al., 2003; Roberts et al., 2014; Rodbell et al., 1999; Tudhope et al., 2001). Given data-model agreement, and armed with our new data compilation, we are now poised to address the question: by what mechanism did insolation dampen ENSO? We review three mechanisms and test whether they are supported by proxy data of tropical Pacific surface and subsurface temperature. We also discuss the implications of June versus September insolation forcing.

5.1. Weaker Upwelling Feedback

One proposed mechanism for Holocene ENSO dampening is weakening of the upwelling feedback, caused by mean warming of the thermocline due to insolation-forced warming of southern subtropical/midlatitude surface waters (Liu et al., 2014; Liu et al., 2000; Roberts et al., 2014). A warmer thermocline, with respect to SST, weakens stratification, decreasing the effect of upwelling on SST and weakening a key positive feedback that generates ENSO (Liu et al., 2014). Thermocline waters in the equatorial Pacific are sourced from surface waters in the subtropics (Hanawa & Talley, 2001) and midlatitudes, with successively deeper layers of the thermocline/subthermocline sourced from successively higher latitudes (Toggweiler et al., 1991). Importantly, about 3 times more water is transported into the equatorial thermocline from the south than from the north (Johnson & McPhaden, 1999) because northern waters are blocked by the Intertropical Convergence Zone (ITCZ) (Johnson & McPhaden, 1999; Lu & McCreary, 1995). These southern subtropical/midlatitude surface waters, centered on 120°W and ~20°S–40°S, subduct during austral winter when the mixed layer deepens (Hanawa & Talley, 2001; Johnson & McPhaden, 1999; O'Connor et al., 2002; Toggweiler et al., 1991; Wong & Johnson, 2003). Therefore, the equatorial thermocline temperature is sensitive to SSTs in the subtropical/midlatitude South Pacific during austral winter and would thus respond to changing June insolation (Liu et al., 2014).

19448007, 2018, 1, Downloaded from https://agupubs.onlinelibrary.wiley.com/doi/10.1002/2017GL075433, Wiley Online Library on [19/07/2025]. See the Terms and Conditions (https://onlinelibrary.wiley.com/terms-and-conditions) on Wiley Online Library for rules of use; OA articles are governed by the applicable Creative Commons License

Another thermocline-based mechanism for dampened early and mid-Holocene ENSO is that changes in insolation weakened the trades in late boreal winter/early spring, allowing westerly wind anomalies to generate downwelling Kelvin waves (Karamperidou et al., 2015). These waves reached the EEP by late summer/early fall and depressed the thermocline, weakening the upwelling feedback and dampening ENSO (Karamperidou et al., 2015). Because modeled trade wind strength is tied to the subtropical highs, which depend on June insolation (Karamperidou et al., 2015; Mantsis et al., 2013), this mechanism, as with the thermocline warming mechanism (Liu et al., 2014), would respond to changes in June insolation.

To test whether the weaker upwelling feedback mechanism is supported by proxy data, we examined tropical Pacific thermocline records. Subsurface temperatures in the EEP and west equatorial Pacific (WEP) show a warmer/deeper thermocline in the early Holocene and cooling toward present (Dang et al., 2012; Sadekov et al., 2013; Xu et al., 2008) (Figure 3b), with weaker EEP stratification in the early and mid-Holocene (data from Sadekov et al., 2013). Subsurface temperatures on the Peru margin were also warmer in the early Holocene (Bova et al., 2015; Kalansky et al., 2015), consistent with evidence for a warmer early and mid-Holocene thermocline in the open ocean. The Karamperidou et al. (2015) mechanism predicts a deeper thermocline only in late summer/early fall, not in the annual average, but this likely aligns with seasonal bias in the proxy record, which emphasizes the upwelling season (Thunell et al., 1983). No proxy records exist from the thermocline source region, but the nearest record (from the Peru margin at 30°S) shows peak SSTs in the early Holocene that cooled toward present (Kaiser et al., 2008), agreeing with equatorial thermocline records. Climate models also show warmer SSTs in the thermocline source region during austral winter/spring in the early and mid-Holocene and show this warm anomaly subducting into the equatorial thermocline (Liu et al., 2014), mirroring modern observations (Wong & Johnson, 2003). Overall, the idea that early and mid-Holocene ENSO dampening resulted from a weaker upwelling feedback due to a warmer/deeper thermocline is well supported.

5.2. Decreased Air-Sea Coupling

Another proposed mechanism for early to mid-Holocene ENSO dampening is that insolation forcing caused cooler SSTs basin-wide, reducing air-sea coupling such that a given SST anomaly produced a smaller atmospheric anomaly, stabilizing ENSO (e.g., An & Choi, 2014). To assess whether cooler SSTs existed basin-wide in the early and mid-Holocene, we created composite SST anomaly records for the WEP and EEP (Figure 3), using published Mg/Ca and alkenone records (see Figures S11 and S12, Table S4, and supporting information for details). In both the EEP and WEP, our Mg/Ca-based SST anomaly records show warmer SST in the early Holocene, contrary to predictions of cooler SST. However, as shown by (Gill et al., 2016), alkenone records diverge from Mg/Ca records in showing cooler early Holocene SST (Figures 3 and S11). While alkenone records support cooler early and mid-Holocene SST, the majority of reconstructions are based on Mg/Ca data and do not show cooler SSTs; as such, there is not clear support for the decreased air-sea coupling hypothesis (e.g., An & Choi, 2014).

5.3. Stronger Walker Circulation

An alternative explanation for Holocene ENSO dampening is that Walker circulation was stronger, either because higher summer/fall insolation created a larger east-west SST difference (Clement et al., 2000; Koutavas & Joanides, 2012; Otto-Bliesner et al., 2003; Sadekov et al., 2013) or because the Asian monsoon and trade winds were stronger (e.g., Braconnot et al., 2012; Bush, 2007). Evidence for a larger east-west SST difference in the early to mid-Holocene is unclear because Mg/Ca and alkenone records disagree in the EEP (Figure 3c). Comparing Mg/Ca data from the WEP and the EEP yields similar east-west SST differences in the early and late Holocene, implying that enhanced Walker circulation cannot explain dampened ENSO in the early Holocene. On the other hand, EEP alkenone data yield a higher east-west SST gradient during the early and mid-Holocene, supporting the Walker circulation hypothesis. However, given the seasonality of alkenone production in the EEP (Leduc et al., 2010; Timmermann et al., 2014), the alkenone SST estimates likely reflect winter conditions, which would not be expected to dampen ENSO (Clement et al., 2000). For clarification, we turn to thermocline tilt, a better indicator of Walker circulation strength than east-west SST difference (DiNezio et al., 2011). Warmer early and mid-Holocene temperatures in both the EEP and WEP thermocline (Dang et al., 2012; Sadekov et al., 2013; Xu et al., 2008) suggest basin-wide warming and/or deepening of the thermocline and do not support a steeper thermocline tilt and strengthened Walker circulation.

19448007, 2018, 1, Downloaded from https://agupubs.onlinelibrary.wiley.com/doi/10.1002/2017GL075433, Wiley Online Library on [19/07/2025]. See the Terms and Conditions (https://onlinelibrary.wiley.com/terms-and-conditions) on Wiley Online Library for rules of use; OA articles are governed by the applicable Creative Commons License

19448007, 2018, 1, Downloaded from https://agupubs.onlinelibrary.wiley.com/doi/10.1002/2017GL075433, Wiley Online Library on [19/07/2025]. See the Terms and Conditions (https://onlinelibrary.wiley.com/terms-and-conditions) on Wiley Online Library for rules of use; OA articles are governed by the applicable Creative Commons License

Our conclusion that the stronger Walker circulation mechanism is not well supported differs from other studies, which argue that changing east-west SST difference does explain variations in ENSO strength (Koutavas & Joanides, 2012; Sadekov et al., 2013). However, Koutavas and Joanides (2012) rely on ENSO being dampened in the mid-Holocene but not early Holocene, contrary to our results, and Sadekov et al. (2013) combine temperature records from the EEP and the eastern tropical Pacific warm pool, which does not represent the EEP or Walker circulation. Overall, considering our new early Holocene ENSO data and SST synthesis, the stronger Walker circulation mechanism is not well supported.

5.4. June Versus September Insolation Forcing

Because September insolation is always higher than June insolation at the equator, it was originally proposed as the driver of long-term changes in ENSO (Clement et al., 2000). Mechanisms that operate entirely within the tropics, including the decreased air-sea coupling and stronger Walker circulation mechanisms, would thus be expected to produce changes in ENSO that follow September insolation timing. However, our finding of dampened ENSO during both the early and mid-Holocene implicates June, not September, insolation as the driver (Figure 3a). June insolation forcing implies an extratropical mechanism of ENSO dampening, supporting the weaker upwelling feedback hypothesis (including changes stemming from mean annual warming or seasonal deepening).

6. El Niño During the Younger Dryas

Our data from 12,170 years B.P., during the YD, show similar El Niño amplitude as the late Holocene. Bioturbation, age uncertainty, and possible changes in sedimentation rate may mean that our sample contains some non-YD specimens; higher-resolution data are needed to confirm our observations. However, our findings are in rough agreement with model results and individual foraminiferal records (Liu et al., 2014; Sadekov et al., 2013), which show slightly stronger ENSO. Similar or strengthened ENSO during the YD cannot be attributed to insolation; instead, it is likely linked to meltwater forcing. Models find that meltwater input to the North Atlantic amplifies ENSO via a southward shift of the ITCZ, which weakens the EEP seasonal cycle and thereby strengthens ENSO via frequency entrainment (Braconnot et al., 2012; Liu et al., 2014; Timmermann et al., 2007). Data showing a southward shift in the ITCZ over the EEP during the YD (e.g., Benway et al., 2006) support this mechanism.

7. Conclusions

Our new Holocene ENSO data and synthesis supports the idea that changing June insolation dampened ENSO during the early and mid-Holocene. This forced evolution of ENSO was likely accompanied by large decadal-centennial variability in ENSO strength, as suggested previously. However, this variability does not preclude a long-term trend, as has been previously argued. The best supported mechanism for early and mid-Holocene ENSO dampening is a weakening of the upwelling feedback, due to insolation-forced mean warming or seasonal deepening of the thermocline. Mechanisms that invoke decreased air-sea coupling and stronger Walker circulation are not well supported by the data. Currently, the effect of stratification and upwelling relative to Walker circulation is a source of disparity among predictions of ENSO under anthropogenic climate change (DiNezio et al., 2012). Given the importance of the upwelling feedback in the Holocene evolution of ENSO, improving its representation in models should be a key target for improving predictions of ENSO behavior.

Acknowledgments
We thank Jean Lynch-Stieglitz and the rest of the MGL1208 shipboard party, Rob Franks for analytical assistance, and Tom Guilderson for radiocarbon analysis. Funding was provided by NSF grants OCE-1405178 and 1204254 and student grants from the Geological Society of America/ExxonMobil and Friends of Long Marine Lab. Our data are deposited at the National Oceanic and Atmospheric Administration National Climatic Data Center. We thank two anonymous reviewers, whose thoughtful comments brought to light some interesting points, and two previous reviewers, whose feedback on an earlier version of this manuscript improved it greatly.

References

An, S.-I., & Choi, J. (2014). Mid-Holocene tropical Pacific climate state, annual cycle, and ENSO in PMIP2 and PMIP3. *Climate Dynamics*, *43*(3-4), 957–970. https://doi.org/10.1007/s00382-013-1880-z

Anand, P., Elderfield, H., & Conte, M. H. (2003). Calibration of Mg/Ca thermometry in planktonic foraminifera from a sediment trap time series. *Paleoceanography*, *18*(2), 1050. https://doi.org/10.1029/2002PA000846

Bard, E., Hamelin, B., Arnold, M., Montaggioni, L., Cabioch, G., Faure, G., & Rougerie, F. (1996). Deglacial sea-level record from Tahiti corals and the timing of global meltwater discharge. *Nature*, *382*(6588), 241–244. https://doi.org/10.1038/382241a0

Benway, H. M., Mix, A. C., Haley, B. A., & Klinkhammer, G. P. (2006). Eastern Pacific warm pool paleosalinity and climate variability: 0–30 kyr. *Paleoceanography*, *21*, PA3008. https://doi.org/10.1029/2005PA001208

Berelson, W. M., Anderson, R. F., Dymond, J., Demaster, D., Hammond, D. E., Collier, R., … Stephens, M. (1997). Biogenic budgets of particle rain, benthic remineralization and sediment accumulation in the equatorial Pacific. *Deep Sea Research Part II: Topical Studies in Oceanography*, *44*(9-10), 2251–2282. https://doi.org/10.1016/S0967-0645(97)00030-1

19448007, 2018, 1, Downloaded from https://agupubs.onlinelibrary.wiley.com/doi/10.1002/2017GL075433, Wiley Online Library on [19/07/2025]. See the Terms and Conditions (https://onlinelibrary.wiley.com/terms-and-conditions) on Wiley Online Library for rules of use; OA articles are governed by the applicable Creative Commons License

Berger, A. L. (1978). Long-term variations of caloric insolation resulting from the Earth's orbital elements. *Quaternary Research*, *9*(02), 139–167. https://doi.org/10.1016/0033-5894(78)90064-9

Bova, S. C., Herbert, T., Rosenthal, Y., Kalansky, J., Altabet, M., Chazen, C., … Zech, J. (2015). Links between eastern equatorial Pacific stratification and atmospheric CO_2 rise during the last deglaciation. *Paleoceanography*, *30*, 1407–1424. https://doi.org/10.1002/2015PA002816

Braconnot, P., Luan, Y., Brewer, S., & Zheng, W. (2012). Impact of Earth's orbit and freshwater fluxes on Holocene climate mean seasonal cycle and ENSO characteristics. *Climate Dynamics*, *38*(5-6), 1081–1092. https://doi.org/10.1007/s00382-011-1029-x

Brown, S. J., & Elderfield, H. (1996). Variations in Mg/Ca and Sr/Ca ratios of planktonic foraminifera caused by postdepositional dissolution: Evidence of shallow Mg-dependent dissolution. *Paleoceanography*, *11*(5), 543–551. https://doi.org/10.1029/96pa01491

Bush, A. B. G. (2007). Extratropical influences on the El Niño–Southern Oscillation through the late Quaternary. *Journal of Climate*, *20*(5), 788–800. https://doi.org/10.1175/jcli4048.1

Carre, M., Sachs, J. P., Purca, S., Schauer, A. J., Braconnot, P., Falcon, R. A., … Lavallee, D. (2014). Holocene history of ENSO variance and asymmetry in the eastern tropical Pacific. *Science*, *345*(6200), 1045–1048. https://doi.org/10.1126/science.1228246

Carton, J. A., & Giese, B. S. (2008). A reanalysis of ocean climate using Simple Ocean Data Assimilation (SODA). *Monthly Weather Review*, *136*(8), 2999–3017. https://doi.org/10.1175/2007mwr1978.1

Chen, S., Hoffmann, S. S., Lund, D. C., Cobb, K. M., Emile-Geay, J., & Adkins, J. F. (2016). A high-resolution speleothem record of western equatorial Pacific rainfall: Implications for Holocene ENSO evolution. *Earth and Planetary Science Letters*, *442*, 61–71. https://doi.org/10.1016/j.epsl.2016.02.050

Chiang, J. C. H., Fang, Y., & Chang, P. (2009). Pacific climate change and ENSO activity in the mid-Holocene. *Journal of Climate*, *22*(4), 923–939. https://doi.org/10.1175/2008jcli2644.1

Christensen, J. H., Kanikicharla, K. K., Marshall, G., & Turner, J. (2013). Climate phenomena and their relevance for future regional climate change. In T. F. Stocker, et al. (Eds.), *Climate Change 2013: The Physical Science Basis. Contribution of Working Group I to the Fifth Assessment Report of the Intergovernmental Panel on Climate Change* (pp. 1217–1308). Cambridge, United Kingdom and New York, NY: Cambridge University Press.

Clement, A. C., Seager, R., & Cane, M. A. (2000). Suppression of El Niño during the mid-Holocene by changes in the Earth's orbit. *Paleoceanography*, *15*(6), 731–737. https://doi.org/10.1029/1999PA000466

Cobb, K. M., Charles, C. D., Cheng, H., & Edwards, R. L. (2003). El Nino-Southern Oscillation and tropical Pacific climate during the last millennium. *Nature*, *424*(6946), 271–276. https://doi.org/10.1038/nature01779

Cobb, K. M., Westphal, N., Sayani, H. R., Watson, J. T., Di Lorenzo, E., Cheng, H., … Charles, C. D. (2013). Highly variable El Nino–Southern Oscillation throughout the Holocene. *Science*, *339*(6115), 67–70. https://doi.org/10.1126/science.1228246

Conroy, J. L., Overpeck, J. T., Cole, J. E., Shanahan, T. M., & Steinitz-Kannan, M. (2008). Holocene changes in eastern tropical Pacific climate inferred from a Galápagos lake sediment record. *Quaternary Science Reviews*, *27*(11-12), 1166–1180. https://doi.org/10.1016/j.quascirev.2008.02.015

Conte, M. H., Sicre, M.-A., Rühlemann, C., Weber, J. C., Schulte, S., Schulz-Bull, D., & Blanz, T. (2006). Global temperature calibration of the alkenone unsaturation index (Uk'37) in surface waters and comparison with surface sediments. *Geochemistry, Geophysics, Geosystems*, *7*, Q02005. https://doi.org/10.1029/2005GC001054

Dang, H., Jian, Z., Bassinot, F., Qiao, P., & Cheng, X. (2012). Decoupled Holocene variability in surface and thermocline water temperatures of the Indo-Pacific warm pool. *Geophysical Research Letters*, *39*, L01701. https://doi.org/10.1029/2011GL050154

de Villiers, S. (2005). Foraminiferal shell-weight evidence for sedimentary calcite dissolution above the lysocline. *Deep Sea Research Part I: Oceanographic Research Papers*, *52*(5), 671–680. https://doi.org/10.1016/j.dsr.2004.11.014

Dekens, P. S., Lea, D. W., Pak, D. K., & Spero, H. J. (2002). Core top calibration of Mg/Ca in tropical foraminifera: Refining paleotemperature estimation. *Geochemistry, Geophysics, Geosystems*, *3*(4), 1022. https://doi.org/10.1029/2001GC000200

DiNezio, P. N., Clement, A., Vecchi, G. A., Soden, B., Broccoli, A. J., Otto-Bliesner, B. L., & Braconnot, P. (2011). The response of the Walker circulation to Last Glacial Maximum forcing: Implications for detection in proxies. *Paleoceanography*, *26*, PA3217. https://doi.org/10.1029/2010PA002083

DiNezio, P. N., Kirtman, B. P., Clement, A. C., Lee, S.-K., Vecchi, G. A., & Wittenberg, A. (2012). Mean climate controls on the simulated response of ENSO to increasing greenhouse gases. *Journal of Climate*, *25*(21), 7399–7420. https://doi.org/10.1175/jcli-d-11-00494.1

Driscoll, R., Eliot, M., Russon, T., Welsh, K., Yokoyama, Y., & Tudhope, A. (2014). ENSO reconstructions over the past 60 ka using giant clams (*Tridacna* sp.) from Papua New Guinea. *Geophysical Research Letters*, *41*, 6819–6825. https://doi.org/10.1002/2014GL061446

Druffel, E. R. M., & Griffin, S. (1993). Large variations of surface ocean radiocarbon: Evidence of circulation changes in the southwestern Pacific. *Journal of Geophysical Research*, *98*(C11), 20249. https://doi.org/10.1029/93JC02113

Duprey, N., Lazareth, C. E., Corrège, T., Le Cornec, F., Maes, C., Pujol, N., … Cabioch, G. (2012). Early mid-Holocene SST variability and surface-ocean water balance in the southwest Pacific. *Paleoceanography*, *27*, PA4207. https://doi.org/10.1029/2012PA002350

Eggins, S., De Deckker, P., & Marshall, J. (2003). Mg/Ca variation in planktonic foraminifera tests: Implications for reconstructing palaeo-seawater temperature and habitat migration. *Earth and Planetary Science Letters*, *212*(3-4), 291–306. https://doi.org/10.1016/s0012-821x(03)00283-8

Elderfield, H., Vautravers, M., & Cooper, M. (2002). The relationship between shell size and Mg/Ca, Sr/Ca, $d^{18}O$, and $d^{13}C$ of species of planktonic foraminifera. *Geochemistry, Geophysics, Geosystems*, *3*(8), 1052. https://doi.org/10.1029/2001GC000194, 1, 13.

Emile-Geay, J., Cane, M., Seager, R., Kaplan, A., & Almasi, P. (2007). El Niño as a mediator of the solar influence on climate. *Paleoceanography*, *22*, PA3210. https://doi.org/10.1029/2006PA001304

Emile-Geay, J., Cobb, K. M., Carré, M., Braconnot, P., Leloup, J., Zhou, Y., … Tudhope, A. (2016). Links between tropical Pacific seasonal, interannual and orbital variability during the Holocene. *Nature Geoscience*, *9*(2), 168–173. https://doi.org/10.1038/ngeo2608

Evans, M. N., Fairbanks, R. G., & Rubenstone, J. L. (1998). The thermal oceanographic signal of El Nino reconstructed from a Kiritimati Island coral. *Journal of Geophysical Research*, *104*, 13,409–13,421.

Faul, K. L., Ravelo, A. C., & Delaney, M. L. (2000). Reconstructions of upwelling, productivity, and photic zone depth in the eastern equatorial Pacific Ocean using planktonic foraminiferal stable isotopes and abundances. *Journal of Foraminiferal Research*, *30*(2), 110–125. https://doi.org/10.2113/0300110

Feely, R. A., Sabine, C. L., Millero, F. J., Langdon, C., Dickson, A. G., Fine, R. A., … Wanninkhof, R. (2008). CLIVAR CO_2 sections P16S_2005 (6 January–19 February 2005) and P16N_2006 (13 February–30 March, 2006). In A. Kozyr (Ed.), *Carbon Dioxide, Hydrographic, and Chemical Data Obtained During the R/Vs Roger Revelle and Thomas G. Thompson Repeat Hydrography Cruises in the Pacific Ocean, O. R. N. L. Carbon Dioxide Information Analysis Center*, Oak ridge, TN: U.S. Department of Energy.

Fehrenbacher, J., Martin, P. A., & Eshel, G. (2006). Glacial deep water carbonate chemistry inferred from foraminiferal Mg/Ca: A case study from the western tropical Atlantic. *Geochemistry, Geophysics, Geosystems*, *7*, Q09P16. https://doi.org/10.1029/2005GC001156

Ford, H. L., Ravelo, A. C., & Polissar, P. J. (2015). Reduced El Nino-Southern Oscillation during the Last Glacial Maximum. *Science*, *347*(6219), 255–258. https://doi.org/10.1126/science.1258437

Fraser, N., Kuhnt, W., Holbourn, A., Bolliet, T., Andersen, N., Blanz, T., & Beaufort, L. (2014). Precipitation variability within the West Pacific warm pool over the past 120 ka: Evidence from the Davao Gulf, southern Philippines. *Paleoceanography*, *29*, 1094–1110. https://doi.org/10.1002/2013PA002599

Gill, E. C., Rajagopalan, B., Molnar, P., & Marchitto, T. M. (2016). Reduced-dimension reconstruction of the equatorial Pacific SST and zonal wind fields over the past 10,000 years using Mg/Ca and alkenone records. *Paleoceanography*, *31*, 928–952. https://doi.org/10.1002/2016pa002948

Hanawa, K., & Talley, L. D. (2001). Mode waters. *International Geophysics Series*, *77*, 373–386. https://doi.org/10.1016/S0074-6142(01)80129-7

Hönisch, B., Allen, K. A., Lea, D. W., Spero, H. J., Eggins, S. M., Arbuszewski, J., … Elderfield, H. (2013). The influence of salinity on Mg/Ca in planktic foraminifers—Evidence from cultures, core-top sediments and complementary $\delta^{18}O$. *Geochimica et Cosmochimica Acta*, *121*, 196–213. https://doi.org/10.1016/j.gca.2013.07.028

Jahnke, R., Heggie, D., Emerson, S., & Grundmanis, V. (1982). Pore waters of the central Pacific Ocean: Nutrient results. *Earth and Planetary Science Letters*, *61*(2), 233–256. https://doi.org/10.1016/0012-821X(82)90056-5

Johnson, G. C., & McPhaden, M. J. (1999). Interior pycnocline flow from the subtropical to the equatorial Pacific Ocean. *Journal of Physical Oceanography*, *29*(12), 3073–3089. https://doi.org/10.1175/1520-0485(1999)029%3C3073:IPFFTS%3E2.0.CO;2

Johnstone, H. J. H., Yu, J., Elderfield, H., & Schulz, M. (2011). Improving temperature estimates derived from Mg/Ca of planktonic foraminifera using X-ray computed tomography-based dissolution index, XDX. *Paleoceanography*, *26*. PA1215. https://doi.org/10.1029/2009PA001902

Kaiser, J., Schefuss, E., Lamy, F., Mohtadi, M., & Hebbeln, D. (2008). Glacial to Holocene changes in sea surface temperature and coastal vegetation in north central Chile: High versus low latitude forcing. *Quaternary Science Reviews*, *27*(21-22), 2064–2075. https://doi.org/10.1016/j.quascirev.2008.08.025

Kalansky, J., Rosenthal, Y., Herbert, T., Bova, S., & Altabet, M. (2015). Southern Ocean contributions to the eastern equatorial Pacific heat content during the Holocene. *Earth and Planetary Science Letters*, *424*, 158–167. https://doi.org/10.1016/j.epsl.2015.05.013

Karamperidou, C., Di Nezio, P. N., Timmermann, A., Jin, F.-F., & Cobb, K. M. (2015). The response of ENSO flavors to mid-Holocene climate: Implications for proxy interpretation. *Paleoceanography*, *30*, 527–547. https://doi.org/10.1002/2014PA002742

Khider, D., Huerta, G., Jackson, C., Stott, L. D., & Emile-Geay, J. (2015). A Bayesian, multivariate calibration for *Globigerinoides ruber* Mg/Ca. *Geochemistry, Geophysics, Geosystems*, *16*, 2916–2932. https://doi.org/10.1002/2015GC005844

Koutavas, A., & Joanides, S. (2012). El Niño-Southern Oscillation extrema in the Holocene and Last Glacial Maximum. *Paleoceanography*, *27*, PA4208. https://doi.org/10.1029/2012PA002378

Leduc, G., Schneider, R., Kim, J. H., & Lohmann, G. (2010). Holocene and Eemian sea surface temperature trends as revealed by alkenone and Mg/Ca paleothermometry. *Quaternary Science Reviews*, *29*(7-8), 989–1004. https://doi.org/10.1016/j.quascirev.2010.01.004

Leduc, G., Vidal, L., Cartapanis, O., & Bard, E. (2009). Modes of eastern equatorial Pacific thermocline variability: Implications for ENSO dynamics over the last glacial period. *Paleoceanography*, *24*, PA3202. https://doi.org/10.1029/2008PA001701

Liu, Z., Kutzbach, J., & Wu, L. (2000). Modeling climate shift of El Nino variability in the Holocene. *Geophysical Research Letters*, *27*(15), 2265–2268. https://doi.org/10.1029/2000GL011452

Liu, Z., Lu, Z., Wen, X., Otto-Bliesner, B. L., Timmermann, A., & Cobb, K. M. (2014). Evolution and forcing mechanisms of El Nino over the past 21,000 years. *Nature*, *515*(7528), 550–553. https://doi.org/10.1038/nature13963

Lu, P., & McCreary, J. P. (1995). Influence of the ITCZ on the flow of thermocline water from the subtropical to the equatorial Pacific Ocean. *Journal of Physical Oceanography*, *25*(12), 3076–3088. https://doi.org/10.1175/1520-0485(1995)025%3C3076:IOTIOT%3E2.0.CO;2

Lynch-Stieglitz, J., Polissar, P. J., Jacobel, A. W., Hovan, S. A., Pockalny, R. A., Lyle, M., … Xie, R. C. (2015). Glacial-interglacial changes in central tropical Pacific surface seawater property gradients. *Paleoceanography*, *30*, 423–438. https://doi.org/10.1002/2014PA002746

Mantsis, D. F., Clement, A. C., Kirtman, B., Broccoli, A. J., & Erb, M. P. (2013). Precessional cycles and their influence on the North Pacific and North Atlantic summer anticyclones. *Journal of Climate*, *26*(13), 4596–4611. https://doi.org/10.1175/jcli-d-12-00343.1

Marchitto, T. M., Muscheler, R., Ortiz, J. D., Carriquiry, J. D., & van Geen, A. (2010). Dynamical response of the tropical Pacific Ocean to solar forcing during the early Holocene. *Science*, *330*(6009), 1378–1381. https://doi.org/10.1126/science.1194887

McGregor, H. V., Fischer, M. J., Gagan, M. K., Fink, D., Phipps, S. J., Wong, H., & Woodroffe, C. D. (2013). A weak El Niño/Southern Oscillation with delayed seasonal growth around 4,300 years ago. *Nature Geoscience*, *6*(11), 949–953. https://doi.org/10.1038/ngeo1936

McGregor, H. V., & Gagan, M. K. (2004). Western Pacific coral $\delta^{18}O$ records of anomalous Holocene variability in the El Niño–Southern Oscillation. *Geophysical Research Letters*, *31*, L11204. https://doi.org/10.1029/2004GL019972

Moy, C. M., Seltzer, G. O., Rodbell, D. T., & Anderson, D. M. (2002). Variability of El Nino-Southern Oscillation activity at millennial timescales during the Holocene epoch. *Nature*, *420*(6912), 162–165. https://doi.org/10.1038/nature01163

O'Connor, B. M., Fine, R. A., Maillet, K. A., & Olson, D. B. (2002). Formation rates of subtropical underwater in the Pacific Ocean. *Deep Sea Research Part I: Oceanographic Research Papers*, *49*(9), 1571–1590. https://doi.org/10.1016/S0967-0637(02)00087-0

Otto-Bliesner, B. L., Brady, E. C., Shin, S.-I., Liu, Z., & Shields, C. (2003). Modeling El Niño and its tropical teleconnections during the last glacial-interglacial cycle, *Geophysical Research Letters*, *30*(23), 2198. https://doi.org/10.1029/2003GL018553

Pausata, F. S. R., Zhang, Q., Muschitiello, F., Lu, Z., Chafik, L., Niedermeyer, E. M., … Liu, Z. (2017). Greening of the Sahara suppressed ENSO activity during the mid-Holocene. *Nature Communications*, *8*, 16020. https://doi.org/10.1038/ncomms16020

Rayner, N. A. (2003). Global analyses of sea surface temperature, sea ice, and night marine air temperature since the late nineteenth century, *Journal of Geophysical Research*, *108*(D14), 4407. https://doi.org/10.1029/2002JD002670

Regenberg, M., Nürnberg, D., Steph, S., Groeneveld, J., Garbe-Schönberg, D., Tiedemann, R., & Dullo, W.-C. (2006). Assessing the effect of dissolution on planktonic foraminiferal Mg/Ca ratios: Evidence from Caribbean core tops. *Geochemistry, Geophysics, Geosystems*, *7*. Q07P15. https://doi.org/10.1029/2005GC001019

Regenberg, M., Regenberg, A., Garbe-Schönberg, D., & Lea, D. W. (2014). Global dissolution effects on planktonic foraminiferal Mg/Ca ratios controlled by the calcite-saturation state of bottom waters. *Paleoceanography*, *29*, 127–142. https://doi.org/10.1002/2013PA002492

Reimer, P. J., Bard, E., Bayliss, A., Beck, J. W., Blackwell, P. G., Ramsey, C. B., … van der Plicht, J. (2013). IntCal13 and Marine13 radiocarbon age calibration curves 0–50,000 years cal BP. *Radiocarbon*, *55*(04), 1869–1887. https://doi.org/10.2458/azu_js_rc.55.16947

Robbins, L. L., Hansen, M. E., Kleypas, J. A., & Meylan, S. C. (2010). CO_2calc—A user-friendly seawater carbon calculator for Windows, Max OS X, and iOS (iPhone), in *U.S. Geological Survey Open-File Report 2010–1280, 17 p.*, edited.

Roberts, W. H. G., Battisti, D. S., & Tudhope, A. W. (2014). ENSO in the mid-Holocene according to CSM and HadCM3. *Journal of Climate*, *27*(3), 1223–1242. https://doi.org/10.1175/jcli-d-13-00251.1

Rodbell, D. T., Seltzer, G. O., Anderson, D. M., Abbott, M. B., Enfield, D. B., & Newman, J. H. (1999). An ~15,000 year record of El Nino-driven alluviation in southwestern Ecuador. *Science*, *283*(5401), 516–520. https://doi.org/10.1126/science.283.5401.516

19448007, 2018, 1, Downloaded from https://agupubs.onlinelibrary.wiley.com/doi/10.1002/2017GL075433, Wiley Online Library on [19/07/2025]. See the Terms and Conditions (https://onlinelibrary.wiley.com/terms-and-conditions) on Wiley Online Library for rules of use; OA articles are governed by the applicable Creative Commons License

Rosenthal, Y., & Lohmann, G. P. (2002). Accurate estimation of sea surface temperatures using dissolution-corrected calibrations for Mg/Ca paleothermometry. *Paleoceanography*, *17*(3), 1044. https://doi.org/10.1029/2001PA000749, 16-1, 16-6.

Rosenthal, Y., Lohmann, G. P., Lohmann, K. C., & Sherrell, R. M. (2000). Incorporation and preservation of Mg in *Globigerinoides sacculifer*: Implications for reconstructing the temperature and $^{18}O/^{16}O$ of seawater. *Paleoceanography*, *15*(1), 135–145. https://doi.org/10.1029/1999PA000415

Sadekov, A. Y., Eggins, S. M., De Deckker, P., Ninnemann, U., Kuhnt, W., & Bassinot, F. (2009). Surface and subsurface seawater temperature reconstruction using Mg/Ca microanalysis of planktonic foraminifera *Globigerinoides ruber*, *Globigerinoides sacculifer*, and *Pulleniatina obliquiloculata*. *Paleoceanography*, *24*. PA3201. https://doi.org/10.1029/2008PA001664

Sadekov, A. Y., Ganeshram, R., Pichevin, L., Berdin, R., McClymont, E., Elderfield, H., & Tudhope, A. W. (2013). Palaeoclimate reconstructions reveal a strong link between El Nino-Southern Oscillation and tropical Pacific mean state. *Nature Communications*, *4*, 2692. https://doi.org/10.1038/ncomms3692

Stott, L., Timmermann, A., & Thunell, R. (2007). Southern Hemisphere and deep-sea warming led deglacial atmospheric CO_2 rise and tropical warming. *Science*, *318*(5849), 435–438. https://doi.org/10.1126/science.1143791

Stuiver, M., & Reimer, P. J. (1993). Extended ^{14}C data base and revised Calib3.0 ^{14}C age calibration program. *Radiocarbon*, *35*(01), 215–230. https://doi.org/10.1017/S0033822200013904

Thirumalai, K., Partin, J. W., Jackson, C. S., & Quinn, T. M. (2013). Statistical constraints on El Niño Southern Oscillation reconstructions using individual foraminifera: A sensitivity analysis. *Paleoceanography*, *28*, 401–412. https://doi.org/10.1002/palo.20037

Thompson, D. M., Conroy, J. L., Collins, A., Hlohowskyj, S. R., Overpeck, J. T., Riedinger-Whitmore, M., … Kannan, M. S. (2017). Tropical Pacific climate variability over the last 6000 years as recorded in Bainbridge Crater Lake, Galápagos. *Paleoceanography*, *32*, 903–922. https://doi.org/10.1002/2017PA003089

Thunell, R. C., Curry, W. B., & Honjo, S. (1983). Seasonal variation in the flux of planktonic foraminifera: Time series sediment trap results from the Panama Basin. *Earth and Planetary Science Letters*, *64*(1), 44–55. https://doi.org/10.1016/0012-821X(83)90051-1

Timmermann, A., Okumura, Y., An, S. I., Clement, A., Dong, B., Guilyardi, E., … Yin, J. (2007). The influence of a weakening of the Atlantic meridional overturning circulation on ENSO. *Journal of Climate*, *20*(19), 4899–4919. https://doi.org/10.1175/jcli4283.1

Timmermann, A., Sachs, J., & Timm, O. E. (2014). Assessing divergent SST behavior during the last 21 ka derived from alkenones and *G. ruber*-Mg/Ca in the equatorial Pacific. *Paleoceanography*, *29*, 680–696. https://doi.org/10.1002/2013PA002598

Toggweiler, J. R., Dixon, K., & Broecker, W. S. (1991). The Peru upwelling and the ventilation of the South Pacific thermocline. *Journal of Geophysical Research*, *96*(C11), 20,467–20,497. https://doi.org/10.1029/91JC02063

Trauth, M. H., Sarnthein, M., & Arnold, M. (1997). Bioturbational mixing depth and carbon flux at the seafloor. *Paleoceanography*, *12*(3), 517–526. https://doi.org/10.1029/97PA00722

Trenberth, K. E. (1997). The definition of El Nino. *Bulletin of the American Meteorological Society*, *78*(12), 2771–2777.

Tudhope, A. W., Chilcott, C. P., McCulloch, M. T., Cook, E. R., Chappell, J., Ellam, R. M., … Shimmield, G. B. (2001). Variability in the El Nino-Southern Oscillation through a glacial-interglacial cycle. *Science*, *291*(5508), 1511–1517. https://doi.org/10.1126/science.1057969

Vetter, L., Spero, H. J., Russell, A. D., & Fehrenbacher, J. S. (2013). LA-ICP-MS depth profiling perspective on cleaning protocols for elemental analyses in planktic foraminifers. *Geochemistry, Geophysics, Geosystems*, *14*, 2916–2931. https://doi.org/10.1002/ggge.20163

Watkins, J. M., Mix, A. C., & Wilson, J. (1996). Living planktic foraminifera: Tracers of circulation and productivity regimes in the central equatorial Pacific. *Deep Sea Research Part II: Topical Studies in Oceanography*, *43*(4-6), 1257–1282. https://doi.org/10.1016/0967-0645(96)00008-2

Wittenberg, A. T. (2009). Are historical records sufficient to constrain ENSO simulations? *Geophysical Research Letters*, *36*, L12702. https://doi.org/10.1029/2009GL038710

Wittenberg, A. T., Rosati, A., Delworth, T. L., Vecchi, G. A., & Zeng, F. (2014). ENSO modulation: Is it decadally predictable? *Journal of Climate*, *27*(7), 2667–2681. https://doi.org/10.1175/jcli-d-13-00577.1

Wong, A. P. S., & Johnson, G. C. (2003). South Pacific eastern subtropical mode water. *Journal of Physical Oceanography*, *33*(7), 1493–1509. https://doi.org/10.1175/1520-0485(2003)033%3C1493:SPESMW%3E2.0.CO;2

Woodroffe, C. D. (2003). Mid-late Holocene El Niño variability in the equatorial Pacific from coral microatolls. *Geophysical Research Letters*, *30*(7), 1358. https://doi.org/10.1029/2002GL015868

Xu, J., Holbourn, A., Kuhnt, W., Jian, Z., & Kawamura, H. (2008). Changes in the thermocline structure of the Indonesian outflow during terminations I and II. *Earth and Planetary Science Letters*, *273*, 152–162. https://doi.org/10.1016/j.epsl.2008.06.029

Zaunbrecher, L. K., Cobb, K. M., Beck, J. W., Charles, C. D., Druffel, E. R. M., Fairbanks, R. G., … Sayani, H. R. (2010). Coral records of central tropical Pacific radiocarbon variability during the last millennium. *Paleoceanography*, *25*, PA4212. https://doi.org/10.1029/2009PA001788

Zhang, Z., Leduc, G., & Sachs, J. P. (2014). El Niño evolution during the Holocene revealed by a biomarker rain gauge in the Galápagos Islands. *Earth and Planetary Science Letters*, *404*, 420–434. https://doi.org/10.1016/j.epsl.2014.07.013

19448007, 2018, 1, Downloaded from https://agupubs.onlinelibrary.wiley.com/doi/10.1002/2017GL075433, Wiley Online Library on [19/07/2025]. See the Terms and Conditions (https://onlinelibrary.wiley.com/terms-and-conditions) on Wiley Online Library for rules of use; OA articles are governed by the applicable Creative Commons License